BULETINUL Universităţii Petrol – Gaze din Ploieşti	Vol. LVIII No. 2 bis / 2006	261-272	Seria Tehnică

Advanced Control of the Electric and Hybrid Vehicles

Iulian Ţopa, Adrian Dănilă, Laurenţiu Diaconu

"Transilvania" University of Braşov,
e-mail: topa@marconi.unitbv.ro

Abstract

In the paper the advanced control of the electric and hybrid vehicles especially for the transmission and the differential is presented. We are focusing on the electrical drives with brushless direct current motors and switched-reluctance motors. The high-grade performance sensorless technologies are used into these applications. The sensorless vector control with modified model reference adaptive system was developed for brushless direct current motors. A method for prediction of rotor position at standstill and rotating shaft conditions in switched reluctance machines is presented in the paper. This method doesn't require additional hardware or memory.

Key words: *electric and hybrid vehicles, adaptive speed controller, brushless d.c. motor, switched reluctance machine.*

Introduction

The development of internal combustion engine vehicles, especially automobiles, is one of the greatest achievements of modern technology. Electric vehicles, hybrid electric vehicles, and fuel cell vehicles have been typically proposed to replace conventional vehicles in the new future [1]-[5].

Electric propulsion systems are the heart of electric vehicles (EVs) and hybrid electric vehicles (HEVs). They consist of electric motors, power converters, and electronic controllers, Figure 1.

Control of DC Motor Drives

Choppers are used for the control of DC motors because of advantages such as high efficiency, flexibility in control, lightweight, small size, quick response, and regeneration down to very low speeds. Presently, the separately excited DC motors are usually used in traction, due to the control flexibility of armature voltage and field.

For DC motor control in open-loop configurations, the chopper offers a number of advantages due to its high operation frequency. High operation frequency results in high frequency output voltage ripple and, therefore, less ripples in the motor armature current and smaller region of discontinuous conduction in the speed-torque plane.

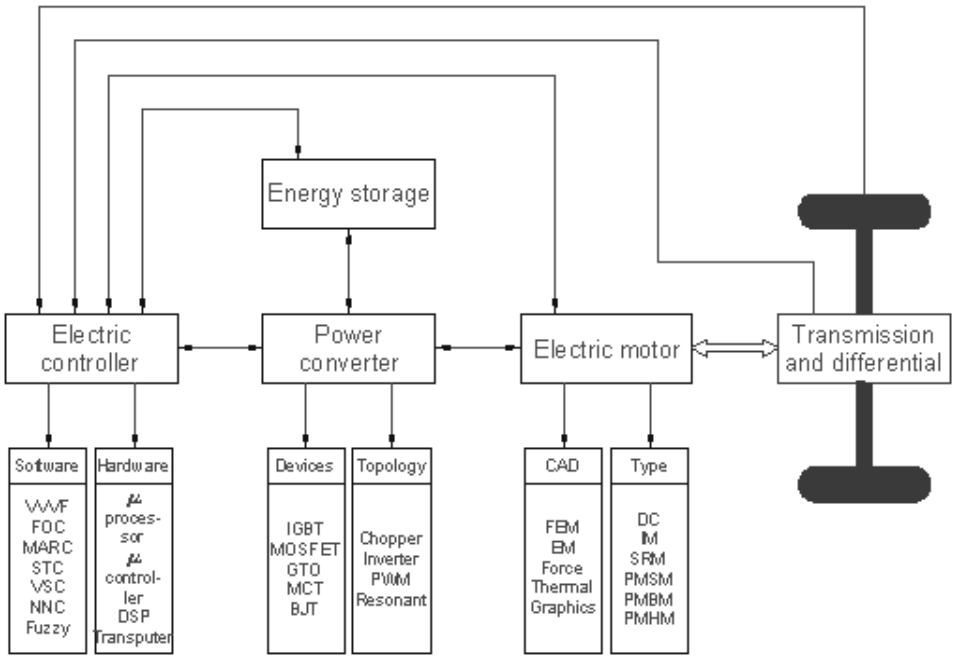

Fig. 1. Functional block diagram of a typical electric propulsion system.

Reduction in the armature current ripple reduces the armature losses. Reduction or elimination of the discontinuous conduction region improves speed regulation and the transient response of the drive. The application of the DC motors on EVs and HEVs requires the motors to operate in multi quadrants, including forward motoring, forward braking, backward motoring, and backward braking.

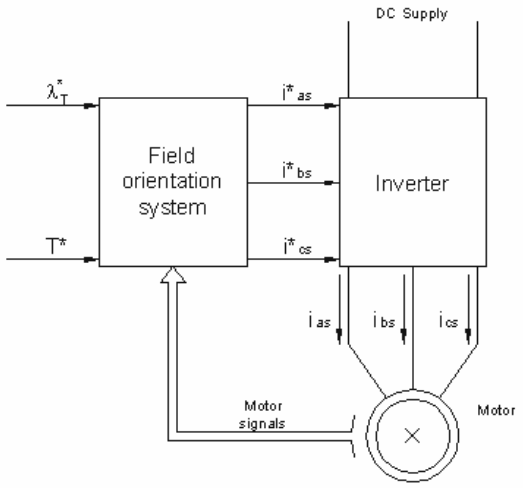

Fig. 2. General block diagram of a vector control system for an induction motor.

Control of Induction Motor Drives

In traction applications with induction motors there are two control principles to be used: constant volt/hertz control and field oriented control. Field oriented control (FOC) or vector control technology, Figure 2, has been successfully developed. This technology mostly overcomes the disadvantages of the constant volt/hertz control in AC motor drives.

Control of Brushless Direct Current (BLDC) Motor Drives

In vehicle traction application, the torque produced is required to follow the torque desired by the driver and commanded through the accelerator and brake pedals. Thus, torque control is the basic requirement. For cruising operation, speed control may be required. Figure 3 shows a block diagram of a torque control scheme for a BLDC through a torque controller.

Many high-performance applications include current feedback for torque control. At the minimum, DC bus current feedback is required to protect the drive and machine from over-currents.

The controller blocks, "speed controller" may be any type of classical controller such as a PI controller, or a more advanced controller such an artificial intelligence control. The "current controller and commutation sequencer" provides the properly sequenced to the "three-phase inverter" while comparing sensed currents to a reference to maintain a constant peak current control.

The operation of the BLDC motor drives relies mostly on position sensors for obtaining the rotor position information so as to perform the turn on or the turn off of each phase properly. Several sensorless technologies have been developed. The majority of them are based on voltage, current, and back EMF detection. These techniques can primarily grouped into four categories:

1. Those using measured currents, voltages, fundamental machine equations, and algebraic manipulations. 2. Those using back EMF methods. Using back EMF sensing is the majority approach in sensorless control technology of the BLDC motor drive. This approach consists of several methods, such as (1) terminal voltage sensing method, (2) third-harmonic back EMF sensing method, (3) freewheeling diode conduction, and (4) back EMF integration.

3. Those using observers. The first of these considered are those utilizing the well-known Kalman filter as position estimator. Other observer-based systems include those utilizing nonlinear, full-order and sliding-mode observers.

4. Those with novel techniques not falling into the previous categories. The first of the novel methods to be considered are those utilizing artificial intelligence, which are the neural networks (ANN) and fuzzy logic. Other techniques consist on detecting the rotor's position by artificial means such as creating artificial saliencies or providing additional stator lamination and using eddy currents effect [6]. The torque observer in [8] was employed to compensate for the feedforward of the position controller. The torque observer was derived from the mechanical dynamic equation with estimated parameters – the mechanical-rotor inertia constant and the friction coefficient [16]. Based on this approach, was proposed a new speed-sensorless approach, witch has a simpler computing algorithm than the estimator-based approaches and is uninfluenced by the time-variant motor parameters or the integrator drift problem, witch difficulties are associated with the back-EMF-based and state observer-based approaches.

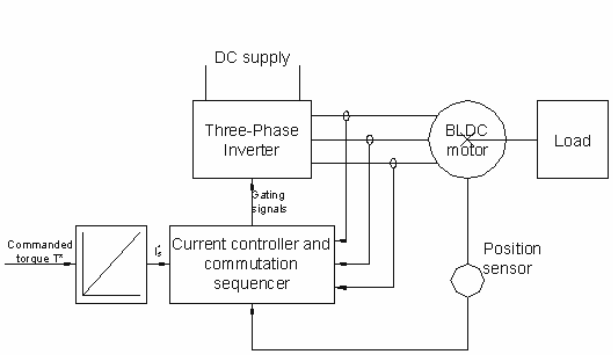

Fig. 3. Block diagram of the torque control of the BLDC motor.

In [9] is reported that the performance of the speed controller influenced the performance of the speed controller influenced the performance of the speed-sensorless approach. Therefore, the

modified model reference adaptive system (MMRAS) [10], an adaptive control algorithm, is used herein in the speed controller of the BLDCM to improve the performance of the speed-sensorless approach. The PI speed controller is used initially and the parameters tuned using the Ziegler-Nichols method [11]–[13] to evaluate the performance of the MMRAS speed controller.

The synchronously rotational reference frame (d-q) axis of the vector control drive is adopted in the study to analyze the BLDCM. The block diagram of speed control loop is presented in Fig. 4.

Both J and B are parameters in the transfer function, witch is the mechanical dynamic equation in Fig. 4. They may vary with the environmental conditions and uncertainties. The recursive least-square (RLS) rule [13], [14] is applied to evaluate the estimated parameters, $\hat{J}$ and $\hat{B}$. And thus increase the robust ness of the system.

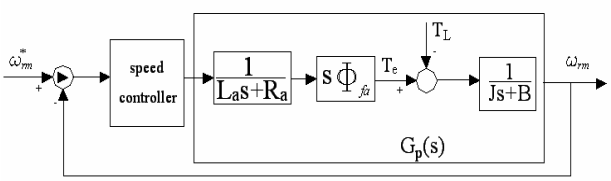

Fig. 4. Block diagram of speed control loop.

Then from inputs $\hat{J}$, $\hat{B}$ and $\hat{\omega}_{rm}$, the torque observer [8] generates the estimated load torque

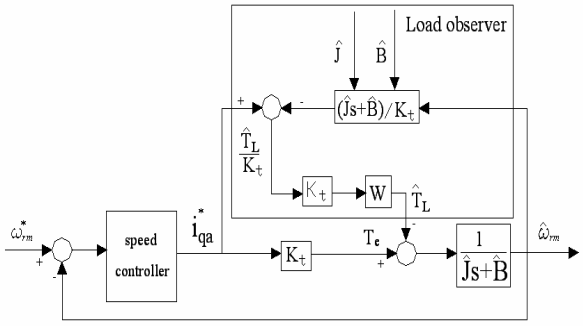

Fig. 5. Sensorless technique with load observer.

($\hat{T}_L$), witch is substituted into the mechanical dynamic equation, to be solved for the mechanical angle rate ($\hat{\omega}_{rm}$). Accordingly, a speed-sensorless technique is developed, as presented in Fig. 5.

Therefore, the proposed sensorless technique is stable, even if the parameters are uncertain load torque varies. Fig. 6 presents the block diagram of the new speed-sensorless vector control for the BLDCM.

The Modified Model Reference Adaptive System (MMRAS), an adaptive control algorithm, is used in the speed controller of the BLDCM, to improve the performance of the speed-sensorless technique. Before the MMRAS is considered, the model reference adaptive system (MRAS) [14]-[16] is described. In responding to a command signal, the MRAS uses a reference model to generate the desired output, which is compared with the actual output of the closed-loop system

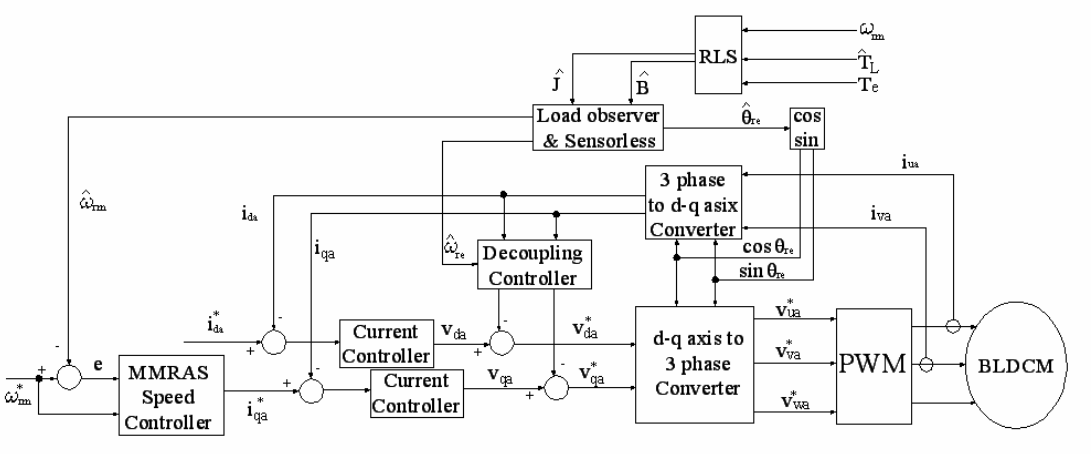

Fig. 6. Sensorless vector control of the BLDCM.

to yield the error signal. Adjusting the parameters in the MRAS subsequently minimizes the error signal.

Based on the speed control loop of the BLDCM in Fig. 4, the plant of the closed-loop system is represented as a second order system

$$G_p(s) = \frac{y(s)}{u(s)} = \frac{c}{s^2 + as + b} \tag{1}$$

where a, b, and c are constants ($a = R_a / L_a + B/J$; $b = R_a * B/(L_a * J)$; $c = s * \phi_{fa} / (L_a * J)$. The reference model of the second order system is then defined as ;

$$G_p(s) = \frac{y_m(s)}{u_c(s)} = \frac{\omega_n^2}{s^2 + 2\xi\omega_n s + \omega_n^2}$$

(2)

where y_m is the reference model output, u_c is the command signal, ξ is the damping ratio, and ω_n is the natural frequency.

The original controller structure in [15] is:

$$u(s) = \theta_1 u_c(s) - \theta_2 y(s) \tag{3}$$

where θ_1 and θ_2 are the adjustable parameters to be evaluated. The controller of the MMRAS algorithm [16] is modified as:

$$u(s) = \theta_1 u_c(s) - \theta_2 e(s) \tag{4}$$

where e is the error and defined as $e = y - y_m$. The difference between (3) and (4) is the feedback signal.)

Finally for updating the controller parameters are obtained :

$$s\theta_1(s) = -\gamma' e(s) \left(\frac{1}{s^2 + as + b} \right) u_c(s) \tag{5}$$

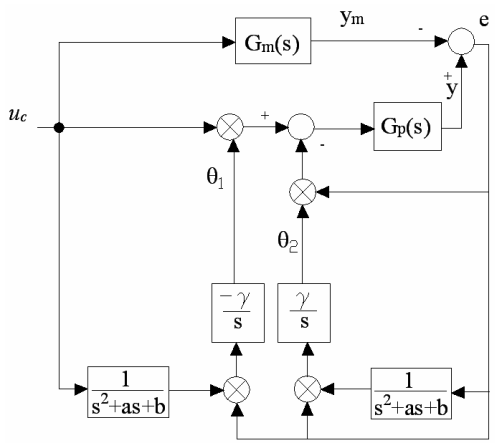

Fig. 7. Block diagram of the MMRAS.

$$s\theta_2(s) = -\gamma' e(s)\left(\frac{1}{s^2 + as + b}\right)e(s) \qquad (6)$$

The block diagram of the MMRAS controller is presented in Fig.7.

The MMRAS was designed to force the plant output to the desired output, enhancing the effect of speed control and improving the performance of the speed-sensorless technique. The PI speed controller, parameters of which are tuned according the Ziegler-Nichols method [11]–[13], are also used to evaluate the performance.

The speed controller uses the MMRAS and PI algorithm, respectively, and their performances are compared.

Fig. 8(a) and (b) present the results of the applying the sensorless algorithm to the motor drive system with the torque observer.

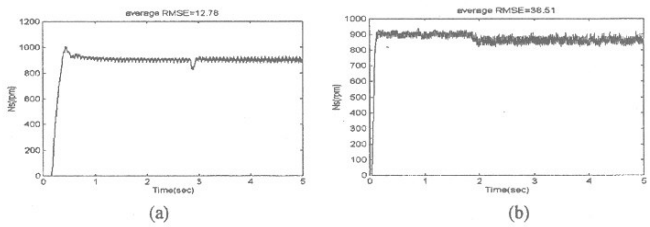

Fig. 8. Simulated speed response of sensorless at 900 rpm under a 0. 0.97-Nm load applied in the middle of the simulation, as determined using (a) MMRAS and (b) PI algorithms.

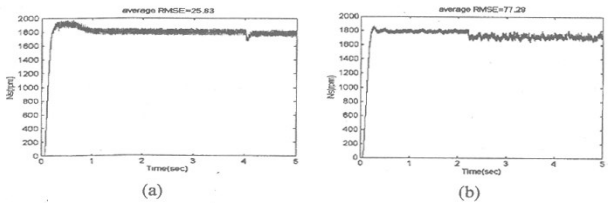

Fig. 9. Experimental speed response of sensor at 1800 rpm with a 0.459 Nm load applied in the middle of the experiment, as determined using (a) MMRAS and (b) PI

Fig.9(a) and (b) plot the experi-mental results obtained at higher speed and under a higher load; the average RMSE values were 25.83 and 77.29, respectively. Clearly, the MMRAS speed controller outperformed the PI speed controller, as revealed by the simulation.

Control of Switched Reluctance Motor Drives

The switched reluctance motor (SRM) drive is considered to be attractive candidate for variable speed motor drives due to its low cost, high power density, rugged structure, reliable converter topology, high efficiency over a wide speed range, and simplicity in control. These drives are suitable for EVs, electric traction applications, automotive applications, aircraft starter/generator systems, mining drives, washing machines, door actuators, etc.

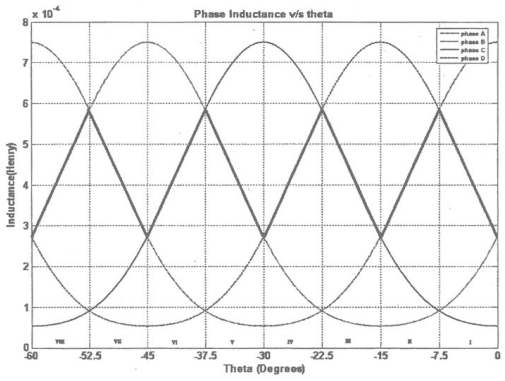

Fig. 11. Inductance profiles of an 8/6 SRM along with the linear segments (solid line).

A conventional SRM drive system consists of the switched reluctance motor, power inverter, sensors such as voltage, current, and position sensors, and control circuitry such as the DSP controller and its peripherals, as shown in figure 10. Through proper control, high performance can be achieved in the SRM drive system.

The SRM drive inverter is connected to a DC power supply.
The torque developed by the motor can be controlled by varying the amplitude and the timing of the current pulses in synchronism with the rotor position.

The input to the SRM drive is DC voltage, which is usually through a front-end diode rectifier or from batteries [7]. Unlike other AC machines, the currents in SR motors can be unidirectional. Hence, conventional bridge inverters used in AC motor drives are not used in SRM drives.
Several sensorless technologies have been developed:

- The Phase Flux Linkage-Based Method: uses phase voltage and current data of the active phases to estimate the rotor position;
- Phase Inductance-Based Method: the essential phase bulk inductance and measured phase current can be input to a stored look-up table storing the functional relation between the phase bulk inductance and phase current and rotor position, to find the corresponding rotor position;
- Modulated Signal Injection Methods: these methods are to apply a voltage to the idle phase winding and measure the resultant phase current to detect the phase inductance. This derived phase inductance will provide the rotor position information;
- Mutually Induced Voltage-Based Method: the idea of this method is based on measuring the mutually induced voltage in an idle phase, which is either adjacent or opposite to the energized phase of an SRM;
- Observer-Based Methods: in this method, state-space equations are used to describe the dynamic behavior of the SRM drive;

The self-tuning techniques are: self-tuning with the Arithmetic Method, self-tuning using an artificial neural network (ANN) ANNs have been successfully used for many applications in control systems.

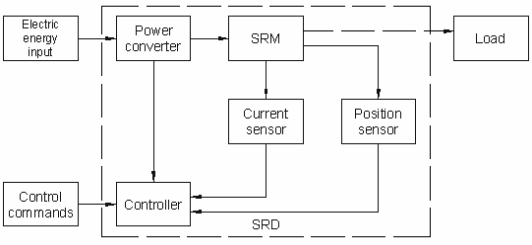

Fig. 10. SRM drive system.

Detection of rotor position at standstill is an essential step in achieving a smooth and reliable startup in sensorless SRM drives.

Ideally, it is desired to obtain precise position information using terminal measurements (i.e., voltages, currents, and time) with no extra hardware or memory.

At standstill, there exists no motional back-emf in a stator phase. This simplifies the phase voltage equation in to the following form (nonlinear effects of saturations not being included):

$$V = ri + L(\theta_0)\frac{di}{dt} \tag{7}$$

where V, r, i, L, and θ_0 stand for phase voltage, stator resistance, phase current, phase inductance, and initial rotor position, respectively. If the rotor is moving, exciting the stator coil with a pulse of voltage will establish a motional back-emf. This changes the differential equation governing the dynamics of the phase to the following from:

$$V = ri + L(\theta)\frac{di}{dt} + \omega i\frac{dL}{d\theta} \tag{8}$$

where θ and ω represent rotor position and the angular velocity of the machine. For sufficiently slow changing systems, the separation between mechanical and electrical responses allows one to assume a constant rotor position during the time when necessary analysis of the diagnostic signals is performed. In order words the phase voltage equation can further be simplified into the following form:

$$V = ri + L(\theta)\frac{di}{dt} + \omega i\frac{dL}{d\theta}\bigg|_{\theta=\theta_0} \tag{9}$$

As one may note in the above equations, the phase inductance (L) contains unique position information. This information can be recovered and decoded into useful position information that is needed for control [17]. The inductance profiles of the stator phases in a SRM are periodic functions of the rotor position. Inductance profile exhibits its maximum and minimum at aligned and unaligned positions respectively. In addition, one may note the existence of the nonlinear regions (flat portions) in the vicinity of the aligned and unaligned positions. Fig. 11 shows the typical unsaturated inductances for an experimental 8/6 SRM. It was noted that there exists a fairly linear region connecting two nonlinear areas for each phase inductance. A close inspection of Fig. 11 indicates that within an electrical cycle of an 8/6 SRM, there exist eight such linear regions. Incorporating these linear segments in the computational process for estimation of the rotor position simplifies the sensorless technique by a significant margin.

Further inspection of the inductance profiles indicates that the division of the profile into eight regions coincides with a unique order of phase inductance magnitude for each region. In other words, by detecting the order of inductance magnitudes among all four phases, one can uniquely detect a region with a length of 7.5^o within which the rotor position is located. This is turn will enable zooming into the targeted region for precise calculation of the rotor angle. These regions, along with the corresponding range of the rotor position and the relationship among the magnitude of inductances are illustrated in Table I.

In order to extract position information, each phase of the stator is excited with a voltage pulse. Once the current in the phase reaches a judiciously selected threshold, the phase voltage is reversed to remove the current and the time required to reach the threshold is recorded. The threshold current is selected such that the resistive drop across the stator resistance can be neglected. At the same time, the threshold current I_{th} is large enough to avoid the undesirable effects of measurement noise and limited resolution in analog to digital conversion.

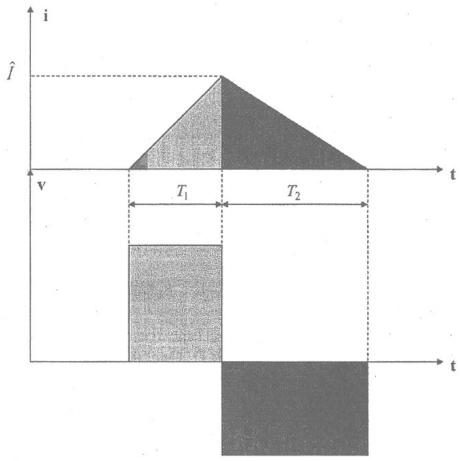

Fig. 12. Diagnostic pulse and associated timing in a rotating rotor case.

The time required for current to reach this threshold is denoted by δ_i, where i denotes the phase order, can be calculated using:

$$\delta \approx L_i(\theta_0)\frac{I_{th}}{V_{dc}}, \quad i=1\ldots4 \tag{10}$$

where I_{th}, V_{dc}, θ_o, and L_i stand for current threshold, effective dc link voltage (after deducting the voltage drop across the semiconductor switches), unknown rotor position, and the respective phase inductance, respectively (I_{th} and V_{dc} are known constants). Equation (10) indicates that the time taken to reach the threshold current is proportional to the phase inductance for each phase. This implies that every region (shown in Fig. 14) can be uniquely detected by comparing the time that is needed in each phase to reach the threshold value. This one to one correspondence is included in Table I. Furthermore, once the regions are detected, a phase with a linear inductance profile can be selected to compute the rotor position. The phase selected for each region is included in the last column of the Table I. One may consider the proposed method as a two step procedure. These steps are:

- identification of the region and phase that should be used for computation of the rotor angle;
- solving the simplified version of the phase voltage equation to obtain the rotor angle with the least amount of computation.

It should be noted that the method can be modified for SRM's with different pole configurations other than 8/6. The phase inductance of the selected phases can be expressed using the following linear approximations:

$$L_k = \{(-1)^k C\}\theta_0 + b_k, \quad k = 1\ldots2m_s \tag{11}$$

where

Table 1
Summary of the partitioning and phase selection used in sensorless technique.

Order of time magnitude	Order of Inductances	Rotor position	Region	Phase chosen
$\delta_1 > \delta_4 > \delta_2 > \delta_3$	$L_1 > L_4 > L_2 > L_3$	0 to -7.5	I	4(D)
$\delta_4 > \delta_1 > \delta_3 > \delta_2$	$L_4 > L_1 > L_3 > L_2$	-7.5 to -15.0	II	1(A)
$\delta_4 > \delta_3 > \delta_1 > \delta_2$	$L_4 > L_3 > L_1 > L_2$	-15 to -22.5	III	3(C)
$\delta_3 > \delta_4 > \delta_2 > \delta_1$	$L_3 > L_4 > L_2 > L_1$	-22.5 to -30.0	IV	4(D)
$\delta_3 > \delta_2 > \delta_4 > \delta_1$	$L_3 > L_2 > L_4 > L_1$	-30.0 to -37.5	V	2(B)
$\delta_2 > \delta_3 > \delta_1 > \delta_4$	$L_2 > L_3 > L_1 > L_4$	-37.5 to -45	VI	3(C)
$\delta_2 > \delta_1 > \delta_3 > \delta_4$	$L_2 > L_1 > L_3 > L_4$	-45 to -52.5	VII	1(A)
$\delta_1 > \delta_2 > \delta_4 > \delta_3$	$L_1 > L_2 > L_4 > L_3$	-52.5 to -60	VIII	2(B)

$$C = \left|\frac{dL_k}{d\theta}\right| \approx \frac{m_s N_r \left(L_{hi} - L_{l0}\right)}{\pi} \tag{12}$$

and

$$b_k = \begin{cases} -k\dfrac{\pi}{m_s N_r} C + L_{hi} & k : \text{odd} \\ k\dfrac{\pi}{m_s N_r} C + L_{l0} & k : \text{even} \end{cases} \tag{13}$$

Furthermore, L_k, L_{hi}, L_{l0}, θ_0, m_s, N_r and k represent inductance of the selected phase, maximum and minimum of the inductance in the linear region (see Fig 11), unknown initial rotor position, number of stator phases, number of rotor poles, and order of the selected region, respectively. By combining (10) and (11), the following equation for detection of the rotor position at standstill is obtained:

$$\left\{(-1)^k C\right\}^{-1} \left\{\frac{V_{dc}}{I_{th}}\delta - b_k\right\} = \theta_0 \tag{14}$$

where δ represents the measured time for the selected phase corresponding to region k (Table I).

In many industrial applications, a quick and smooth engagement of SR drives to the mechanical load is demanded. Automotive power steering and starter/alternators are among applications where such flexibility is required. These necessitates the capability to detect the rotor position at rotating shaft condition and subsequent engagement of a position sensorless control.

Owing to the existence of nonzero velocity, injection of diagnostic signals results in the generation of an induced motional back emf in the stator coils. Neglecting the resistive drop, one can rewrite the phase voltage equation (9) for a sufficiently small duration of time as follows:

$$V = L(\theta_0)\frac{di}{dt} + \omega i \left.\frac{dL}{d\theta}\right|_{\theta=\theta_0} \tag{9a}$$

It is assumed that the speed of calculation in the detection routine is sufficiently fast so the incremental movement of the rotor can be neglected. In order to detect the region within which the rotor position is located, the same diagnostic approach is used as in the standstill case. If the angular velocity of the drive is large enough then the time required for the current to reach the threshold (T_1 in Fig. 12) and the time required for removal of current (T_2) will be different.

By comparing the duration of the diagnostic pulses in each phase one can uniquely detect the region in which the rotor position is currently resides. As can be seen from Fig. 11 each region there are two phases in the motoring mode (positive slope) and the other two are in the generating mode of operation (negative slope). If a particular phase is in the generating mode of operation then we have

$$T_1 < T_2 \tag{15}$$

Similarly, for motoring case

$$T_2 < T_1 \tag{16}$$

These inequalities reflect the impact of motional back-emf on the rise and fall of the diagnostic current. During generation, the motional back-emf would accelerate the build up of the current and would slow down its removal (15). During motoring, the motional back-emf opposes the

rise of the current and accelerates the removal of the current (16). In order to detect the proper region within witch the rotor position is located a voltage pulse is applied to each stator phase. By measuring the rise and fall times (T_1 and T_2) for each phase and using (15) and (16) the region of interest can be detected. In each region, one of the phases has a linear relationship between inductance and rotor position. This phase will be used for computation of the rotor angle. In order to compute the rotor angle, lets consider (14) in the neighborhood of $t = T_1$ (Fig. 11). One can approximate (14) in the vicinity of this point as given by:

$$V_{dc} \cong \left\{ L(\theta_0)\frac{I_{th}}{T_1} + (-1)^k C\omega I_{th} \right\}\Bigg|_{t=T_1-\varepsilon} \tag{17}$$

in which ε is an incrementally small positive number. By subtracting both sides of these two equations in (17) and using (11) one can show that the estimated rotor position can be given by

$$\hat{\theta}_0 = \left\{(-1)^k C\right\}^{-1}\left\{ \frac{2V_{dc}T_1T_2}{I_{th}(T_1+T_2)} - b_k \right\} \tag{18}$$

One may note that (14) represents a special case of (17) when T_1 and T_2 are equal. It is also important to note that this calculation is only valid if by completion of the above process the total displacement of the rotor is negligible. Fig. 13 illustrates the measured rotor position as compared to the actual positions. The estimated and measured rotor position at 20 rpm are illustrated in Fig. 14. It can be see from the comparative plots that a respectable match has been achieved although the noise caused by digital to analog converter and some inaccuracy in transition from one sensing phase to another was also observed.

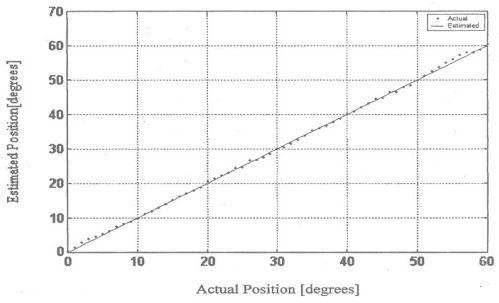

Fig. 13. Detected versus actual positions at standstill condition.

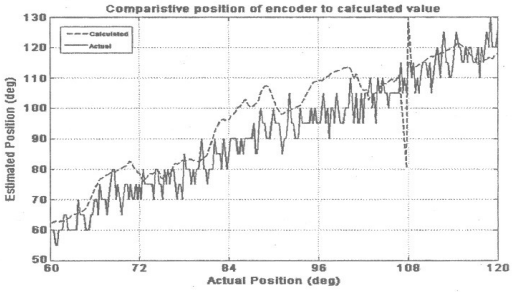

Fig. 14. Comparison of the estimated and measured rotor position under rotating shaft conditions (speed=20

This method eliminates the problem of starting hesitation. Besides, it also offers adequate accuracy and requires no additional hardware or memory. In addition, the proposed method is relatively easy to implement and can be easily modified to fit SRMs with different pole configurations. These make the proposed technique very practical, reliable and cost-effective, and suitable for implementation in mass-manufactured products-domestic and industrial areas alike.

References

1. Husain, I. - *Minimization of torque ripple in SRM drives*, IEEE Transactions on Industrial Electronics, no. 49, pp. 28-39, 2002.
2. Rahman, K. M. and Ehsani, M. - *Performance analysis of electrical motor drives for electric and hybrid electric vehicle application*, IEEE Power Electronics In Transportation, pp. 49-56, Nov.1996.

3. Senjyu, T. and Uezato, K. - Adjustable speed control of brushless DC motor with out position and speed sensors, in *Proceedings of the IEEE/IAS Conf. On Industrial Automation and Control: Emerging Technologies*, pp. 160-164, 1995.
4. Ehsani, M., Gao, Y., Gay, S. E. and Emadi, A. - *Modern electric, hybrid electric, and fuel cell Vehicles*, CRC Press, London, 2005.
5. Miller, T. J. E. - *Switched Reluctance Motors and their Control*, Oxford Science Publications, London, 1993.
6. Huang, F. and Tien, D. - *A neural network approach to position sensor-less control of brushless DC motors*, in Proceedings of the IEEE 22nd International Conference on Industrial Electronics, Control, and Instrumentation, Vol. 2, pp. 1167-1170, Aug. 1996.
7. Mohan, N., Undeland, T. M., and Robbins, W. P. - *Power Electronics – Converters, Applications, and Design*, John Wiley & Sons, New York, 1995.
8. Lin, F. J. - *Real-time IP position controller design with torque feedforward control of PM synchronous motor*, IEEE Trans. Ind. Electron., vol. 44, no. 6, pp. 398-407, Dec. 1997.
9. Lin, J. M., Wang, H. P., and Lin, M. C. - *LEQG/LTR controller design with extended Kalman filter for sensorless induction motor servo drive*, IEECE Trans. Fundamentals, vol. E82-A, no. 12, pp. 2793-2801, 1999.
10. Wang, H. P., Chen, G. Z., and Ni, L. T. - *The controller with error feedback for modified model reference adaptive system*, J. Constr. Syst. Technol., vol. 6, no. 4, pp. 283-286, 1998.
11. Åström, K. J., and Hägglund, T. - *Auto-matic Tuning of PID Controllers,* Instrument Society of America, New York, 1998.
12. Ziegler, J. G., and Nichols, N. B. - *Optimum settings for automatic controllers*, Trans. ASME, vol. 64, pp. 759-768, 1942.
13. Häng, C. C., Åström, K. J, and Ho, W. K. - *Refinement of the Ziehler Nichols tuning formula*, Proc. Inst. Electr. Eng., vol. 138, no. 2, pp. 111-118, 1991.
14. Mareels, I., and Polderman, J. W. - *Adaptive Systems: An Introduction,* MA: Birkhäuser, Boston, 1996.
15. Åström, K. J. and Wittenmark, B. - *Adaptive control,* 2nd ed. Reading, MA: Addison-Wesley, 1995.
16. Wang, H.p., and Liu, Y.T. - *Integrated Design of Speed-sensorless and Adaptive Speed Controller for a Brushless DC Moto*r, In IEEE Transactions on Power Electronics , Vol. 21, no. 2, pp. 518-523,2006.
17. Edrington, C.S., and Fahimi, B. - *Prediction of Rotor Position at Standstill and Rotating Shaft Conditions in Switched Reluctance Machines,* In IEEE Transaction on Power Electronics, Vol. 21, pp. 225-233, 2006.

Reglarea avansată a vehiculelor electrice şi hibride

Rezumat

In aceasta lucrare este prezentata reglarea avansata in special ale transmisiei si diferentialului vehiculelor electrice si hibride. Lucrarea se concentreaza asupra actionarilor electrice cu motoare de curent continuu fara perii si motoare sincrone cu reluctanta variabila. In cadrul acestor aplicatii se utilizeaza reglarea tehnologiile avansate de reglare fara senzori. Reglarea vectoriala fara senzori cu sistem adaptiv cu model de referinta modificat a fost dezvoltata pentru motoarele de curent continuu fara perii. In aceasta lucrare este prezentata o metoda de predictie a pozitiei rotorului in repaus si miscare de rotatie pentru masinile cu reluctanta variabila. Aceasta metoda nu necesita capacitati hardware sau de memorie suplimentare.